

Non-linear Integrated Sachs-Wolfe effect

Asantha Cooray

*Department of Astronomy and Astrophysics, University of Chicago, Chicago, Illinois 60637.
 Sherman Fairchild Senior Research Fellow, California Institute of Technology, Pasadena, California 91125.
 E-mail: asante@hyde.uchicago.edu*

(Submitted to PRD)

We discuss the non-linear extension to the integrated Sachs-Wolfe effect (ISW) resulting from the divergence of the large scale structure momentum density field. The non-linear ISW effect leads to an increase in the total ISW contribution by roughly two orders of magnitude at $l \sim 1000$. This increase, however, is still below the cosmic variance limit of the primary anisotropies; at further small angular scales, secondary effects such as gravitational lensing and the kinetic Sunyaev-Zel'dovich (SZ) effect dominates the non-linear ISW power spectrum. We show this second-order non-linear ISW contribution is effectively same as the contribution previously described as a lensing effect due to the transverse motion of gravitational lenses and well known as the Kaiser-Stebbins effect under the context of cosmic strings. Due to geometrical considerations, there is no significant three point correlation function, or a bispectrum, between the linear ISW effect and its non-linear extension. The non-linear ISW contribution can be potentially used as a probe of the transverse velocity of dark matter halos such as galaxy clusters. Due to the small contribution to temperature fluctuations, of order few tenths of micro Kelvin, however, extracting useful measurements on velocities will be challenging.

I. INTRODUCTION

It is by now well known the importance of cosmic microwave background (CMB) temperature fluctuations as a probe of cosmology [1]. The accuracy to which cosmological information can be extracted depends on how well we understand individual processes that lead to anisotropies in CMB temperature. Though effects during recombination are now well understood [2], contributions and modifications to CMB anisotropies due to large scale structure between last scattering surface and today is not completely well established. This is primarily due to the non-linear evolution of the large scale structure at low redshifts such that simple analytical calculations based on linear theory may no longer be applicable. In general, large scale structure affects CMB through two processes: gravity and Compton scattering. The modifications due to gravity arises from frequency changes via gravitational red and blue-shifts, while during the reionized epoch, photons can both generate and erase primary fluctuations through scattering via free electrons.

Here, we discuss an effect due to gravitational redshift commonly known in the literature as the integrated Sachs-Wolfe (ISW; [3]) effect at late times.¹ The temperature fluctuations in the ISW effect results from the differential redshift effect from photons climbing in and out of time evolving potential perturbations from last scattering surface to present day. In currently popular cold dark matter cosmologies with a cosmological constant, significant contributions arises at redshifts less than 1 and on and above the scale of the horizon at the time of decay.

Here, in particular, we extend previous discussions on the ISW effect, usually due to linear fluctuations in the density field, to the non-linear regime of clustering. The non-linear contribution to ISW effect is generally called the Rees-Sciama (RS; [4]) effect, though such a distinction is arbitrary since temperature fluctuations in CMB arise essentially due to time evolving potentials in both the linear and non-linear regime of fluctuations. Using the continuity equation, we show that the non-linear contributions to ISW effect comes from the divergence of the large scale structure momentum density field. We model the large scale structure momentum density field using the recently popular halo model where large scale structure density field fluctuations can be described through dark matter within halos and correlations between halos [5,6]. Our analytical calculations are consistent with those of [7] based on numerical simulations.

In addition to a recalculation of the contribution, we also discuss this non-linear extension to the ISW effect under the context of proposed contributions to CMB temperature in the literature. We show the non-linear ISW contribution is essentially same as temperature anisotropy produced through the transverse motions of foreground gravitational lenses as was first discussed in Ref. [8] and with further discussions and corrections in Ref. [9]. The effect is generally

¹To avoid confusion, we distinguish contributions to ISW effect during matter dominant era as late ISW effect, though there is an additional contribution during the radiation dominance.

called the moving lens contribution [10,11] and its cosmic string analogue is the well known Kaiser-Stebbins effect [12]. Under this lensing description, the effect can be described as the gravitational lensing of the CMB dipole, formed by the transverse motion of a halo or a galaxy cluster, in the rest frame the halo. We show that there is no significant non-Gaussian correlations associated with the non-linear ISW effect and the bispectrum formed with linear effects are negligible. There is also no correlation between the kinetic SZ effect, due to the momentum density field along the line of sight, and the non-linear ISW effect.

The layout of the paper is as follows. In § II, we outline the non-linear contribution to the ISW effect after reviewing briefly background material relevant for current calculations in the context of the adiabatic cold dark matter (CDM) models. In § III, we discuss our results and consider the non-linear contribution under the context of suggested secondary effects in CMB. We also discuss the bispectrum formed by the combined linear ISW and its non-linear extension. In the same section, we study the possibility for an extraction of the transverse velocity of galaxy clusters using the non-linear ISW effect.

II. CALCULATIONAL METHOD

We first review the properties of adiabatic CDM models relevant to the present calculations.

A. Adiabatic CDM Model

The expansion rate for adiabatic CDM cosmological models with a cosmological constant is

$$H^2 = H_0^2 [\Omega_m(1+z)^3 + \Omega_K(1+z)^2 + \Omega_\Lambda] , \quad (1)$$

where H_0 can be written as the inverse Hubble distance today $H_0^{-1} = 2997.9h^{-1}\text{Mpc}$. We follow the conventions that in units of the critical density $3H_0^2/8\pi G$, the contribution of each component is denoted Ω_i , $i = c$ for the CDM, g for the baryons, Λ for the cosmological constant. We also define the auxiliary quantities $\Omega_m = \Omega_c + \Omega_b$ and $\Omega_K = 1 - \sum_i \Omega_i$, which represent the matter density and the contribution of spatial curvature to the expansion rate respectively.

Convenient measures of distance and time include the conformal distance (or lookback time) from the observer at redshift $z = 0$

$$r(z) = \int_0^z \frac{dz'}{H(z')} , \quad (2)$$

and the analogous angular diameter distance

$$d_A = H_0^{-1} \Omega_K^{-1/2} \sinh(H_0 \Omega_K^{1/2} r) . \quad (3)$$

Note that as $\Omega_K \rightarrow 0$, $d_A \rightarrow r$ and we define $r(z = \infty) = r_0$.

In linear theory, the density field may be scaled backwards to higher redshift by the use of the growth function $G(z)$, where $\delta(k, r) = G(r)\delta(k, 0)$ [13]

$$G(r) \propto \frac{H(r)}{H_0} \int_{z(r)}^\infty dz' (1+z') \left(\frac{H_0}{H(z')} \right)^3 . \quad (4)$$

Note that in the matter dominated epoch $G \propto a = (1+z)^{-1}$.

Although we maintain generality in all derivations, we illustrate our results with the currently favored Λ CDM cosmological model. The parameters for this model are $\Omega_c = 0.30$, $\Omega_b = 0.05$, $\Omega_\Lambda = 0.65$, $h = 0.65$, $Y_p = 0.24$, $n = 1$, $X = 1$, with a normalization such that mass fluctuations on the $8h \text{ Mpc}^{-1}$ scale is $\sigma_8 = 0.9$, consistent with observations on the abundance of galaxy clusters [14] and COBE normalization [15]. A reasonable value here is important since higher order correlations is nonlinearly dependent on the amplitude of the density field. To compute the linear power spectrum, we adopt the fitting formula for the transfer function given in [16].

B. ISW effect

The integrated Sachs-Wolfe effect [3] results from the late time decay of gravitational potential fluctuations. The resulting temperature fluctuations in the CMB can be written as

$$T^{\text{ISW}}(\hat{\mathbf{n}}) = -2 \int_0^{r_0} dr \dot{\Phi}(r, \hat{\mathbf{n}}r), \quad (5)$$

where the overdot represent the derivative with respect to conformal distance (or equivalently look-back time). Writing multipole moments of the temperature fluctuation field $T(\hat{\mathbf{n}})$,

$$a_{lm} = \int d\hat{\mathbf{n}} T(\hat{\mathbf{n}}) Y_l^{m*}(\hat{\mathbf{n}}), \quad (6)$$

we can formulate the angular power spectrum as

$$\langle a_{l_1 m_1}^* a_{l_2 m_2} \rangle = \delta_{l_1 l_2}^D \delta_{m_1 m_2}^D C_{l_1}. \quad (7)$$

For the ISW effect, multipole moments are

$$a_{lm}^{\text{ISW}} = i^l \int \frac{d^3 \mathbf{k}}{2\pi^2} \int dr \dot{\Phi}(\mathbf{k}) I_l(k) Y_l^m(\hat{\mathbf{k}}), \quad (8)$$

with $I_l(k) = \int dr W^{\text{ISW}}(k, r) j_l(kr)$, and the window function for the ISW effect, W^{ISW} (see below). The angular power spectrum is then given by

$$C_l^{\text{ISW}} = \frac{2}{\pi} \int k^2 dk P_{\dot{\Phi}\dot{\Phi}}(k) [I_l(k)]^2, \quad (9)$$

where the three-dimensional power spectrum of the time-evolving potential fluctuations are defined as

$$\langle \dot{\Phi}(\mathbf{k}_1) \dot{\Phi}(\mathbf{k}_2) \rangle = (2\pi)^3 \delta_D(\mathbf{k}_1 + \mathbf{k}_2) P_{\dot{\Phi}\dot{\Phi}}(k_1). \quad (10)$$

The above expression for the angular power spectrum can be evaluated efficiently under the Limber approximation [17] for sufficiently high l values, usually in the order of few tens, as

$$C_l^{\text{ISW}} = \int dr \frac{[W^{\text{ISW}}]^2}{d_A^2} P_{\dot{\Phi}\dot{\Phi}} \left[k = \frac{l}{d_A}, r \right]. \quad (11)$$

In order to calculate the power spectrum of time-derivative of potential fluctuations, we make use of the cosmological Poisson equation [18]. In Fourier space, we can relate the fluctuations in the potential to the density field as:

$$\Phi = \frac{3}{2} \frac{\Omega_m}{a} \left(\frac{H_0}{k} \right)^2 \left(1 + 3 \frac{H_0^2}{k^2} \Omega_K \right)^{-2} \delta(k, r). \quad (12)$$

Thus, the derivative of the potential can be related to a derivative of the density field and the scale factor a . Considering a flat universe with $\Omega_K = 0$, we can write the full expression for the power spectrum of time-evolving potential fluctuations, as necessary for the ISW effect valid in all regimes of density fluctuations, as

$$P_{\dot{\Phi}\dot{\Phi}}(k, r) = \frac{9}{4} \left(\frac{\Omega_m}{a} \right)^2 \left(\frac{H_0}{k} \right)^4 \times \left[\left(\frac{\dot{a}}{a} \right)^2 P_{\delta\delta}(k, r) - 2 \frac{\dot{a}}{a} P_{\delta\dot{\delta}}(k, r) + P_{\dot{\delta}\dot{\delta}}(k, r) \right], \quad (13)$$

with $W^{\text{ISW}} = -2$ in equations 9 and 11.

To calculate the power spectrum involving the correlations between time derivatives of density fluctuations, $P_{\dot{\delta}\dot{\delta}}$, and the cross-correlation term involving the density and time-derivative of the density fields, $P_{\delta\dot{\delta}}$, we make use of the continuity equation, which in position, or real, space can be written in the form:

$$\dot{\delta}(\mathbf{x}, r) = -\nabla \cdot [1 + \delta(\mathbf{x}, r)] \mathbf{v}(\mathbf{x}, r). \quad (14)$$

In the linear regime of fluctuations, when $\delta(\mathbf{x}, r) = G(r)\delta(\mathbf{x}, 0) \ll 1$, the time derivative is simply $\dot{\delta}^{\text{lin}}(\mathbf{x}, r) = -\nabla \cdot \mathbf{v}(\mathbf{x}, r)$ and we can obtain the well-known result for linear theory velocity fluctuations in Fourier space as

$$\mathbf{v} = -i\dot{G}\delta(k, 0)\frac{\mathbf{k}}{k^2}. \quad (15)$$

Thus, in linear theory, $P_{\delta\dot{\delta}} \equiv k^2 P_{vv}(k, r) = \dot{G}^2 P_{\delta\delta}^{\text{lin}}(k, 0)$ and $P_{\delta\dot{\delta}} \equiv k P_{\delta v}(k, r) = G\dot{G} P_{\delta\delta}^{\text{lin}}(k, 0)$

These lead to the well-known results for the linear ISW effect, with a power spectrum for $\dot{\Phi}$ as

$$P_{\dot{\Phi}\dot{\Phi}}^{\text{lin}}(k, r) = \frac{9}{4} \left(\frac{\Omega_m}{a} \right)^2 \left(\frac{H_0}{k} \right)^4 \left[-\frac{\dot{a}}{a} G(r) + \dot{G} \right]^2 P_{\delta\delta}^{\text{lin}}(k, 0). \quad (16)$$

The term within the square bracket is \dot{F}^2 where $F = G/a$ following derivation for the linear ISW effect in [19]. Even though, we have replaced the divergence of the velocity field with a time-derivative of the growth function, it should be understood that the contributions to the ISW effect comes from the divergence of the velocity field and not directly from the density field. Thus, to some extent, even the linear ISW effect reflects statistical properties of the large scale structure velocities.

In the mildly non-linear to fully non-linear regime of fluctuations, the approximation in equation 14, involving $\delta \ll 1$, is no longer valid and a full calculation of the time-derivative of density perturbations is required. This can be achieved in the second order perturbation theory, though, such an approximation need not be fully applicable as the second order perturbation theory fails to describe even the weakly non-linear regime of fluctuations exactly. Motivated by applications of the halo approach to large scale structure [5,6] and results from numerical simulations [20], we consider a description for the time-derivative of density fluctuations and rewrite equation 14 as

$$\dot{\delta}(\mathbf{x}, r) = -\nabla \cdot \mathbf{v}(\mathbf{x}, r) - \nabla \cdot \delta(\mathbf{x}, r) \mathbf{v}(\mathbf{x}, r), \quad (17)$$

where we have separated the momentum term involving $p = (1 + \delta)v$ to a velocity contribution and a density velocity product. In Fourier space,

$$\begin{aligned} \dot{\delta}(\mathbf{k}) &= i\mathbf{k} \cdot p(\mathbf{k}) \\ &= i\mathbf{k} \cdot \mathbf{v}(\mathbf{k}) + \int \frac{d^3\mathbf{k}'}{(2\pi)^3} \delta(\mathbf{k} - \mathbf{k}') i\mathbf{k} \cdot \mathbf{v}(\mathbf{k}'), \end{aligned} \quad (18)$$

where we have dropped the time-dependence for clarity. The first term involving the velocity field leads to the linear theory ISW effect, while the non-linear aspects are captured in the term involving convolution of the δv term (see, also [7]). Following the approach motivated by Hu in Ref. [21], discussed by Cooray in Ref. [6] and investigated in detail through numerical simulations by Sheth et al. in Ref. [20], we can write the power spectrum of density derivatives, or equivalently the divergence of the momentum density field, as

$$\begin{aligned} P_{\delta\dot{\delta}}(k) &\equiv k^2 P_{pp}(k) \\ &= k^2 P_{vv}^{\text{lin}}(k) + k^2 \int \frac{d^3\mathbf{k}'}{(2\pi)^3} \mu'^2 P_{\delta\delta}(|\mathbf{k} - \mathbf{k}'|) P_{vv}(k') \\ &\quad + k^2 \int \frac{d^3\mathbf{k}'}{(2\pi)^3} \frac{(k - k'\mu')\mu'}{|\mathbf{k} - \mathbf{k}'|} P_{\delta v}(|\mathbf{k} - \mathbf{k}'|) P_{\delta v}(k') \\ &\quad + k^2 \int \frac{d^3\mathbf{k}'}{(2\pi)^3} \int \frac{d^3\mathbf{k}''}{(2\pi)^3} \mu' \mu'' T_{\delta\delta vv}(\mathbf{k} - \mathbf{k}', -\mathbf{k} - \mathbf{k}'', \mathbf{k}', \mathbf{k}''). \end{aligned} \quad (19)$$

In the non-linear regime, $\mathbf{k} - \mathbf{k}' \sim \mathbf{k}$ and $\mathbf{k} - \mathbf{k}'' \sim \mathbf{k}$ and we can simplify by integrating over angles to obtain,

$$P_{\delta\dot{\delta}} = k^2 P_{vv}^{\text{lin}}(k) + \frac{1}{3} k^2 P_{\delta\delta}(k) \int \frac{k'^2 dk'}{2\pi^2} P_{vv}(k'). \quad (20)$$

Note that in the deeply non-linear regime, contribution from the trispectrum formed by the velocity-density correlations drop out; this is due to the fact that under the halo approach, the non-linear trispectrum resulting from the

single halo term is independent of the configuration and thus, not on μ' and μ'' (see, discussions in [6] and [22]). Also, the term involving product of cross-power spectra between the density and velocity fields does not contribute in the non-linear regime; at small scales, the density fluctuations are independent of the large scale velocity field. In figure 1, we show the power spectrum of momentum divergence, which in linear theory is simply described by the divergence of the velocity field, with the extension to the non-linear regime of fluctuations following equation 20.

Our description of the non-linear momentum power spectrum is similar to the derivation of the non-linear kinetic SZ effect in Hu [21] and Cooray [6] (see, also, [20]) which involves the momentum field along the line of sight. In equation 20, the integral over the velocity power spectrum is simply the RMS of the velocity fluctuations

$$v_{rms}^2 = \int dk \frac{P_{\delta\delta}^{lin}(k)}{2\pi^2}. \quad (21)$$

Thus, the non-linear power spectrum of the momentum field divergence, as relevant for the ISW effect, involves one of three components of the velocity field with $1/3v_{rms}^2$; note that the expression for the fully non-linear contribution to the momentum field along the line of sight is similar to above and also involves one component of the velocity field as discussed in [21] and [6]. The resulting expression for the non-linear momentum field is fully consistent with simulations [20].

In addition to the power spectrum of density derivatives, in equation 13, we also require the cross power spectrum between density derivatives and density field itself $P_{\delta\delta}$. In [20], using the halo approach as a description of the momentum density field observed in simulations, it was found that the cross-correlation between the density field and the momentum field can be well described as

$$P_{p\delta}(k) = \sqrt{P_{pp}(k)P_{\delta\delta}(k)}. \quad (22)$$

This is equivalent to the statement that the density and momentum density fields are perfectly correlated with a cross-correlation coefficient of 1; this relation is exact at mildly-linear scales while at deeply non-linear scales this perfect cross-correlation requires mass independent peculiar velocity for individual halos [20]. Using this observation, we make the assumption that $P_{\delta\delta} \sim \sqrt{P_{\delta\delta}P_{\delta\delta}}$, which is generally reproduced under the halo model description of the cross-correlation between density field and density field derivatives. This cross-term leads to a 10% reduction of power at multipoles between 100 and 1000, when compared to the total when linear and non-linear contributions are simply added.

III. DISCUSSION

In figure 2, we show the angular power spectrum of the ISW effect with its non-linear extension (which we have labeled RS for Rees-Sciama effect). The curve labeled ISW effect is the simple linear theory calculation with a power spectrum for potential derivatives given in equation 16. The curves labeled “lin” and “nl” shows the full non-linear calculation following the description given in equation 13 and using the linear theory or full non-linear power spectrum, in equation 20, for the density field, respectively. For the non-linear density field power spectrum, we make use of the halo approach for large scale structure clustering [5,6] and calculate the power spectrum through a distribution of dark matter halos. We use linear theory to describe the velocity field in both linear and non-linear cases; since the velocity field only contributes as an overall normalization, through v_{rms} , its non-linear effects, usually at high k values, are not important due to the shape of the velocity power spectrum and the behavior of the integral in equation 21.

As shown in figure 2, the overall correction due to the non-linear ISW effect leads roughly two orders of magnitude increase in power at $l \sim 1000$. The difference between linear and non-linear theory density field power spectrum in equation 20, only leads to at most an order of magnitude change in power. Note that the curve labeled “lin” agrees with previous second order perturbation theory calculations of the Rees-Sciama effect [7], while the curve labeled “nl” is also consistent with previous estimates based on results from numerical simulations.

There is an additional feature that should be observed in figure 2, but not properly described previously in the literature. At $l \sim 100$ to 1000, there is roughly a 10% decrease in total power from what is generally described in the literature as the Rees-Sciama contribution. This is due to the $P_{\delta\delta}$ term in equation 13. If one simply adds the linear ISW and non-linear RS contributions, this cross-correlation term is not present. This dip, due to a cancellation, is present when comparing results based on perturbation theory for RS and numerical simulations for the full non-linear ISW effect (see, [7]); The cross term provides a natural explanation for the slight decrease in power.

In figure 3, we break the contribution to the non-linear effect, without the linear ISW or cross-term contributions, as a function of steps in redshift. As shown, one essentially finds equal contributions over a wide range in redshift with most of the contributions coming from a redshift ~ 1 to multipoles of few hundred where the power peaks.

Even though there is roughly two orders of magnitude increase in power at multipoles around 1000, in figure 4, we show that this increase is still below the cosmic variance associated with primary contribution given by

$$\Delta C_l = \sqrt{\frac{2f_{\text{sky}}^{-1}}{2l\Delta_l + \Delta_l^2}} C_l^{\text{CMB}}, \quad (23)$$

where Δ_l is the bin size in multipole space and f_{sky} is the fraction of sky covered. The signal-to-noise for the detection of the power spectrum is

$$\left(\frac{S}{N}\right)^2 = \frac{f_{\text{sky}}}{2} \sum_l (2l+1) \left(\frac{C_l}{C_l^n}\right)^2, \quad (24)$$

where C_l^n is the power spectrum of noise with $C_l^n = C_l^{\text{CMB}} + C_l^{\text{s}} + C_l^{\text{det}}$; C_l^{s} is any contribution from secondary effects and C_l^{det} is any detector noise contribution. As shown in figure 4(b), the cumulative signal-to-noise is less than one even for a full sky experiment with $f_{\text{sky}} = 1$ and no detector noise. Here, we include contributions from the thermal and kinetic Sunyaev-Zel'dovich effects (SZ; [23,6]) and lensing effect on CMB [24] as secondary contributions to the noise power spectrum. The top line with cumulative signal-to-noise slightly above one is when thermal SZ effect is removed from the noise contribution.

Given the significant sample variance and the fact that the non-linear ISW effect has no special property, such as a different frequency spectrum from thermal CMB as in the case of thermal SZ effect [23,25], it is unlikely that the non-linear ISW effect power spectrum can be extracted from CMB data easily. Going to much smaller angular scales, or large multipoles, leads to a reduction in the cosmic variance, though, increase in power associated with other small angular scale secondary effects such as the thermal SZ effect or the kinetic SZ effect can complicate any detection of the non-linear ISW effect. Later, we will address the possibility whether, instead of statistical properties such as the power spectrum or the bispectrum (see below), we can extract the associated signal from individual objects such as massive galaxy clusters.

A. ISW Bispectrum

Following our earlier discussion for the angular power spectrum, we can also consider the bispectrum (see, [26]), or the Fourier analog of the three point correlation function:

$$\begin{aligned} B(\hat{\mathbf{n}}, \hat{\mathbf{m}}, \hat{\mathbf{l}}) &\equiv \langle T(\hat{\mathbf{n}})T(\hat{\mathbf{m}})T(\hat{\mathbf{l}}) \rangle \\ &\equiv \sum \langle a_{l_1 m_1} a_{l_2 m_2} a_{l_3 m_3} \rangle Y_{l_1}^{m_1}(\hat{\mathbf{n}}) Y_{l_2}^{m_2}(\hat{\mathbf{m}}) Y_{l_3}^{m_3}(\hat{\mathbf{l}}), \end{aligned} \quad (25)$$

where the sum is over $(l_1, m_1), (l_2, m_2), (l_3, m_3)$. Statistical isotropy again allows us to express the correlation in terms of an m -independent function,

$$\langle a_{l_1 m_1} a_{l_2 m_2} a_{l_3 m_3} \rangle = \begin{pmatrix} l_1 & l_2 & l_3 \\ m_1 & m_2 & m_3 \end{pmatrix} B_{l_1 l_2 l_3}. \quad (26)$$

Here the quantity in parentheses is the Wigner-3j symbol. The orthonormality relation for Wigner-3j symbol implies

$$B_{l_1 l_2 l_3} = \sum_{m_1 m_2 m_3} \begin{pmatrix} l_1 & l_2 & l_3 \\ m_1 & m_2 & m_3 \end{pmatrix} \langle a_{l_1 m_1} a_{l_2 m_2} a_{l_3 m_3} \rangle. \quad (27)$$

For the coupling between ISW effects, using multipolar moments written in equation 8, we can write the bispectrum as

$$\begin{aligned} B_{l_1 l_2 l_3} &= \sqrt{\frac{(2l_1+1)(2l_2+1)(2l_3+1)}{4\pi}} \begin{pmatrix} l_1 & l_2 & l_3 \\ 0 & 0 & 0 \end{pmatrix} \\ &\times b_{l_1, l_2, l_3}, \end{aligned} \quad (28)$$

with

$$\begin{aligned}
b_{l_1, l_2, l_3} &= \frac{2^3}{\pi^3} \int k_1^2 dk_1 \int k_2^2 dk_2 \int k_3^2 dk_3 \\
&\times B_{\dot{\Phi}\dot{\Phi}\dot{\Phi}}(k_1, k_2, k_3) I_{l_1}(k_1) I_{l_2}(k_2) I_{l_3}(k_3) \\
&\times \int x^2 dx j_{l_1}(k_1 x) j_{l_2}(k_2 x) j_{l_3}(k_3 x).
\end{aligned} \tag{29}$$

As before, Limber approximation [17] allows one to simplify the integrals for speedy calculation

$$\begin{aligned}
b_{l_1, l_2, l_3} &= \int dr \frac{W^{\text{ISW}}(k_1, r) W^{\text{ISW}}(k_2, r) W^{\text{ISW}}(k_3, r)}{d_A^4} \\
&\times B_{\dot{\Phi}\dot{\Phi}\dot{\Phi}}(k_1, k_2, k_3) \Big|_{k_1=\frac{l_1}{d_A}, k_2=\frac{l_2}{d_A}, k_3=\frac{l_3}{d_A}}.
\end{aligned} \tag{30}$$

Similar to the power spectrum in equation 10, the three dimensional bispectrum of the derivatives of potential fluctuations are defined as

$$\begin{aligned}
\langle \dot{\Phi}(k_1) \dot{\Phi}(k_2) \dot{\Phi}^{\text{nl}}(k_3) \rangle &= (2\pi)^3 \delta_D(\mathbf{k}_1 + \mathbf{k}_2 + \mathbf{k}_3) \\
&\times B_{\dot{\Phi}\dot{\Phi}\dot{\Phi}}(k_1, k_2, k_3)
\end{aligned} \tag{31}$$

As an approximation, this three-dimensional bispectrum can be calculated in second order perturbation theory (e.g., [27]). To obtain an exact result valid both in the weakly non-linear and non-linear regimes, we consider the coupling between two linear ISW effects and the non-linear extension involving the $\nabla \cdot \delta \mathbf{v}$ term. This leads to a bispectrum following:

$$\begin{aligned}
B_{\dot{\Phi}\dot{\Phi}\dot{\Phi}}(k_1, k_2, k_3) &= -\frac{27}{8} \left(\frac{\Omega_m}{a} \right)^3 \frac{H_0^6}{k_1^2 k_2^2 k_3^2} \left[-\frac{\dot{a}}{a} G + \dot{G} \right]^2 \\
&\times G \dot{G} \left[P_{\delta\delta}(k_1, 0) P_{\delta v}(k_2, 0) \frac{\mathbf{k}_3 \cdot \mathbf{k}_2}{k_2} + \text{Perm.} \right],
\end{aligned} \tag{32}$$

where permutations are with respect to the ordering of $\mathbf{k}_1, \mathbf{k}_2$ and \mathbf{k}_3 leading to a total of six terms. In equation 30, $W^{\text{ISW}} = -2$ as defined earlier. Because of the dependence on an angle, say $\mathbf{k}_3 \cdot \mathbf{k}_2$ in $B_{\dot{\Phi}\dot{\Phi}\dot{\Phi}}(k_1, k_2, k_3)$, there is significant cancellations and the final projected angular bispectrum of the ISW effect is smaller than a simple order of magnitude estimate involving the cube of the temperature fluctuation amplitude. In figure 7, we show the cumulative signal-to-noise for the ISW bispectrum, with

$$\left(\frac{S}{N} \right)^2 = f_{\text{sky}} \sum_{l_1, l_2, l_3} \frac{B_{l_1 l_2 l_3}^2}{6 C_{l_1}^n C_{l_2}^n C_{l_3}^n}, \tag{33}$$

where again the noise power spectrum is C_l^n (see, Ref. [19] for details). In figure 7, we take $C_l^n = C_l^{\text{CMB}}$ to consider sample variance from primary anisotropies alone. The cumulative signal-to-noise is in the order of few times 10^{-7} , suggesting that the bispectrum is unlikely to be detected; similar values are also found for other three point statistics such as the skewness or the third moment. Thus, consistent with the second order perturbation theory result [27], there is no significant non-Gaussian signal at the three-point level formed by the correlation between linear ISW effects and the non-linear ISW effect in the non-linear regime of fluctuations. Also note that there is no bispectrum of the form $\langle \dot{\Phi}(k_1) \dot{\Phi}^{\text{nl}}(k_2) \dot{\Phi}^{\text{nl}}(k_3) \rangle$ since such a term leads to an odd number of velocity or density fluctuation terms.

B. Cross-Correlations

An additional way to extract or detect the presence of this signal is through cross-correlations with another source of anisotropy or a tracer of large scale structure. Since the momentum density field is involved in the non-linear ISW effect, one can expect the presence of a correlation between another tracer of the momentum density field. It is well known that the kinetic SZ effect traces the line of sight large scale structure momentum density field such that the temperature fluctuations can be written as a modulation of the velocity field by baryon fluctuations

$$T^{\text{kSZ}}(\hat{\mathbf{n}}) = \int dr g(r) \hat{\mathbf{n}} \cdot \mathbf{v}(r, \hat{\mathbf{n}} r) \delta_b(r, \hat{\mathbf{n}} r), \tag{34}$$

where δ_b is the fluctuation in the baryon field and $g(r)$ is a weight function for Compton-scattering with $g \equiv \dot{\tau}e^{-\tau} = XH_0 0.0691(1 - Y_p)\Omega_g h(1+z)^2 e^{-\tau}$ where $\tau(r) = \int_0^r dr \dot{\tau}$ is the optical depth out to r [28,19,6].

The correlation between the non-linear ISW effect and the kinetic SZ effect is then

$$\langle a_{l_1 m_1}^{*, \text{ISW}} a_{l_2 m_2}^{\text{kSZ}} \rangle \propto \int \frac{d^3 \mathbf{k}'}{(2\pi)^3} \mu' \sqrt{1 - \mu'^2} P_{\delta b}(\mathbf{k}) P_{vv}(\mathbf{k}'), \quad (35)$$

and is equal to zero through the angular terms involving the integral over $\mathbf{k} \cdot \mathbf{k}' = kk'\mu'$; the cross-correlation involves a cosine term from the divergence of the momentum associated with non-linear ISW effect and a sine term from the line of sight momentum associated with the kinetic SZ effect. The geometrical cancellation is merely a statement that though locally line of sight velocity field may be correlated with its transverse component, on average over the whole sky, there is no such correlation. This cancellation can be avoided by several techniques. In [6], we discussed a similar situation involving the cross-correlation between the thermal SZ effect and the kinetic SZ effect and suggested the use of a quadratic correlation involving the square of the density field. This is also equivalent to the use of absolute values of the temperature fluctuations.

C. Relation to other effects

We now suggest the non-linear extension to the ISW effect is essentially the same contribution described by [8] using transverse motion of lensing objects; under the context of cosmic strings, this contribution is well known as the Kaiser-Stebbins effect [12]. Writing, $T(\hat{\mathbf{n}}) = \int dr \Delta T(r\hat{\mathbf{n}}, r)$, we consider the ISW effect such that $\Delta T(r\hat{\mathbf{n}}, r) = -2\dot{\Phi}(r)$. Following our earlier discussion related to the non-linear contribution, we can relate the potential fluctuations to the density fluctuations using the Poisson equation. The contributions now follow as $\Delta T \propto [-\dot{a}/a\delta + \dot{\delta}]$. The first term containing the time-derivative of the scale factor was recently reintroduced by [29] as a time-delay effect. As discussed in [30], the time-delay contribution to CMB is second order as it involves a product of the spatial gradient of CMB at the last scattering surface and the cumulative time-delay contribution and is not simply described by a first order contribution. Additionally, as discussed for the linear ISW effect, only considering the \dot{a} term leads to an overestimate of the fluctuation as there is a cancellation from a first order term involving the $\dot{\delta}$ term.

As before, using the complete continuity equation, we can relate the time derivative of the density fluctuations, $\dot{\delta}$, to the divergence of the velocity field and the divergence of the product of density overdensity and velocity $\Delta T \propto [\dot{a}/a\delta + \nabla \cdot (1 + \delta)\mathbf{v}]$. Here, we consider the non-linear contribution resulting from the $\Delta T^{\text{nl}} \propto \nabla \cdot \delta\mathbf{v}$ term and reintroducing the density field in terms of potentials using the Poisson equation,

$$\begin{aligned} \Delta T^{\text{nl}} &= -2\nabla \cdot (\Phi\mathbf{v}) \\ &\approx -\mathbf{v}_\perp \cdot (2\nabla_r \Phi) \\ &= -v \sin \alpha \delta_{\text{len}} \cos \phi. \end{aligned} \quad (36)$$

The simplifications assume that potential fluctuations are embedded in a velocity field with much larger coherence scale so that gradients in the velocity field do not contribute to temperature anisotropies. Furthermore, we have introduced the lensing deflection angle $\delta_{\text{len}} = 2\nabla_r \Phi$ where the gradient is now an angular gradient on the sky and there is no contribution to temperature anisotropy from the gradient of potential along the line of sight. This forces the contributing component of the velocity field to be the one on the sky and not along the line of sight. Here, α is the angle between the line of sight and the velocity field and ϕ is the position angle from the observer. As it is now clear, this latter description of the non-linear ISW effect is what has been provided elsewhere under the context of moving gravitational lenses [10,11].

The correspondence between the two effects can also be noted using the the description which is well utilized to calculate the gravitational lensing effect on CMB [24,19,31]. Writing,

$$\begin{aligned} T(\hat{\mathbf{n}}) &= T(\hat{\mathbf{n}} + \Delta\hat{\mathbf{n}}) \\ &= T^{\text{P}}(\hat{\mathbf{n}}) + \nabla_r T^{\text{P}}(\hat{\mathbf{n}}) \cdot \Delta\hat{\mathbf{n}}, \end{aligned} \quad (37)$$

where angular deflections due to gravitational lensing follows such that $\Delta\hat{\mathbf{n}} = 2\nabla_r \phi$, where the projected lensing potential is $\phi(\hat{\mathbf{n}}) = D_{ls}/D_s \Phi$. Here, $T^{\text{P}}(\hat{\mathbf{n}})$ is the primary CMB contribution while $\nabla_r T^{\text{P}}(\hat{\mathbf{n}})$ is the angular gradient on the sky of these temperature fluctuations. Essentially, gravitational lensing angular deflections remap the distribution of temperature fluctuations and this remapping is captured by the dependence on distances where distance from lens to source (CMB last scattering surface) is D_{ls} and the distance from observer to source is D_s . Also, as written,

gravitational lensing effect on CMB is second order due to the dependence on the angular gradient of the CMB on the sky, $\nabla_r T$; this is consistent with the fact that lensing does not change the surface brightness and only results in a modification of the temperature fluctuation distribution.

The second order effect related to non-linear ISW effect is due to the lensing of the dipole created by the motion of halos such that $\nabla_r T = v \sin \alpha$. To be consistent with the description given under the time-derivative of the density fluctuations, we require $D_{ls} = D_s$, such that there is no dependence on the ratio of distance factors, usually encountered in lensing studies. This is equivalent to the case that $D_l \ll D_s$ such that $D_{ls} \sim D_s$, which is not necessarily true even for clusters at $z \sim 0.5$. In either case, the non-linear ISW effect cannot be considered as a remapping of the temperature fluctuations similar to the conventional gravitational lensing, as there is no real source, a temperature gradient, in the problem; the temperature gradient essentially exists from the coordinate transformation from a moving lens to a stationary lens². The inconsistency with lensing mapping description arises, unfortunately, when attempting to describe the contribution from the divergence of the momentum density field as a gravitational lensing effect.

D. Towards transverse velocities

As discussed before, the detection of the power spectrum of temperature anisotropies due to the non-linear ISW effect is heavily affected by the dominant cosmic variance of CMB primary anisotropies. Due to geometrical considerations, there is also no significant non-Gaussian contribution or a cross-correlation with other effects. Thus, instead of statistical properties such as the power spectrum, one can try to extract the associated signal in individual objects such as massive galaxy clusters.

In figure 5, we show the distinct signature formed by the non-linear ISW effect for a cluster of mass $5 \times 10^{14} M_\odot$ with a transverse velocity of 100 km sec^{-1} across the line of sight. We assume a NFW [32] profile for the dark matter distribution of the cluster and take a description for the concentration mass relation following [33]. In terms of the density distribution of the cluster, the deflection angle, at an impact distance of η from the cluster center, is given by

$$\delta_{\text{len}}(\eta) = \frac{8\pi G}{c^2 \eta} \int_0^\eta r_\perp dr_\perp \sum(r_\perp) \quad (38)$$

where the surface mass density is

$$\sum(r_\perp) = \int_{-r_v}^{+r_v} dr_\parallel \rho(r_\perp, r_\parallel). \quad (39)$$

In above, r_\perp is the distance across the line of sight, r_\parallel is the distance along the line of sight and r_v is the virial radius of the cluster, which we take to be at an overdensity of 200 following the NFW [32] description. Above equation for the deflection angle also assumes a circularly-symmetric dark matter distribution within the halo.

As shown in figure 5, the contribution to temperature fluctuations are at most $0.3 \mu\text{K}$. In order to detect this small signal, one has to be able to extract it from other contributions to CMB due to galaxy clusters. The most significant contributions from clusters arise from the SZ thermal effect [23] due to inverse-Compton scattering of photons via hot electrons. Here, temperature changes of order 1 mK is produced and these are now routinely observed towards massive clusters [34]. The SZ thermal effect, however, has a distinct frequency dependence and in multifrequency CMB data, the effect can be separated out from thermal CMB and other fluctuations [25]. The next significant contribution comes from kinetic SZ effect due to the line of sight motion of the scatterers in clusters [23]. In figure 6, we show the kinetic SZ effect for the same cluster as in figure 5. Here, we have assumed that the electron distribution in clusters is described by the hydrostatic equilibrium [6] and have taken a line of sight velocity of 100 km sec^{-1} . The contribution due to the SZ kinetic effect, and also SZ thermal effect, is highly peaked towards the center of the cluster and can be as high as few tens μK .

The next important contribution is due to gravitational lensing of the large scale CMB gradient, whose rms is of order $13 \mu\text{K arcmin}^{-1}$. With a deflection angle of order ~ 0.5 arcmins, the contribution due to lensing is in the range of few μK . As shown in figure 6, the lensing effect has the same profile shape as the contribution resulting from the transverse velocity; the two profiles need not lie in the same direction since the large scale CMB gradient

²We note that this issue has led to some confusion in the literature when calculating the so-called moving lens effect with some including the ratio of D_{ls}/D_s [10] while others, correctly, not [11]

and the transverse velocities can be aligned differently. When the thermal SZ effect is separated, in temperature fluctuations, a galaxy cluster exhibits a slight offsetted dipolar pattern with a significant temperature increment or decrement towards the center, resulting from the direction of the line of sight velocity associated with the kinetic SZ effect. Detecting such a profile will certainly remain a challenging goal for the future cluster observations [35].

Eventually, if the transverse velocity contribution can be detected, its amplitude and the direction of the dipole pattern, provides significant information on large scale structure velocities not generally available from other observations. We can ask how well one can detect a typical cluster through this effect. First, to make a reasonable signal-to-noise detection, it is clear that one must extract effects such as the kinetic SZ and CMB lensing. This requires detailed knowledge on the baryon and dark matter distributions within clusters. Assuming such information is available, we can obtain an estimate for the signal-to-noise by noting that the observed signal can be written as [35,36]

$$\frac{\Delta T}{T}(\theta) = s(\theta) + n(\theta), \quad (40)$$

where $s(\theta)$ is the profile of the signal and $n(\theta)$ is the profile of the noise distribution. In order to remove the excess noise associated with large scale temperature fluctuations from primary anisotropies or other secondary effects, we can construct an appropriately normalized filter which provides an optimal detection of the signal in the presence of such noise. This filter can be written as

$$\Psi(\mathbf{l}) = \frac{s(\mathbf{l})}{C_l^n} \left[\int \frac{d^2\mathbf{l}}{(2\pi)^2} \frac{|s(\mathbf{l})|^2}{C_l^n} \right]^{-1} \quad (41)$$

where C_l^n is the power spectrum of noise. The signal to noise for the detection of the profile, for an axi-symmetric distribution for $s(\theta)$, is

$$\left(\frac{S}{N} \right)^2 = \int \frac{l dl}{2\pi} \frac{s(l)^2}{C_l^n}. \quad (42)$$

In figure 8, we show the cumulative signal-to-noise, as a function of l . Here, we assume a noise power spectrum given by the sum of the intrinsic CMB and secondary effects, where secondary effects include all thermal contributions: CMB lensing, kinetic SZ and a model for the inhomogeneous reionization. At small l 's, corresponding to outer extent of the cluster, fluctuations in the intrinsic CMB temperature confuse the detection of the signal while at large l 's, corresponding to inner extent of the cluster, fluctuations from local universe complicate. Even if detailed properties of clusters are known so that intrinsic CMB lensing and the kinetic SZ effect can be perfectly separated from the transverse effect, it is unlikely that we will not know all sources of temperature fluctuations along the line of sight towards a given cluster leading to a confusion in the detection. For typical transverse velocities of order few 100 km sec⁻¹, we find signal-to-noise values of order 0.1 suggesting that detection of this signal for individual clusters will remain challenging even for an experiment with no instrumental noise contributions; alternatively, one can put an upper limit on the transverse velocity contribution at the level of few thousand km sec⁻¹; this upper limit is considerably larger than what one expects under currently popular Λ CDM cosmological models.

The signal-to-noise for detection may be improved if cross-correlation techniques can be considered, for e.g., if one has some knowledge on the intrinsic and secondary fluctuations towards the observed cluster and has some knowledge on the direction of the large scale bulk flows from other methods, even if amplitude of that bulk flow is not known. Separately, since the coherence scale of bulk flows are much larger than an individual cluster, it may be possible to extract the transverse effect by averaging the signal over a number of clusters. Using numerically simulated cluster images, and realistic sources of noise and confusions, we plan to study how well such an extraction can be performed in a future paper.

IV. SUMMARY

We have discussed the non-linear extension to the integrated Sachs-Wolfe effect (ISW) resulting from the divergence of the large scale structure momentum density field. This non-linear ISW effect, calculated under the recently popular halo approach to non-linear large scale structure clustering, leads to an increase in the total ISW contribution by roughly two orders of magnitude at $l \sim 1000$. This increase, however, is still below the cosmic variance limit of the primary anisotropies; at further small angular scales, secondary effects such as gravitational lensing and the kinetic Sunyaev-Zel'dovich (SZ) effect dominates the non-linear ISW power spectrum.

Further, we have shown that this second-order non-linear ISW contribution is effectively same as the contribution previously described as a lensing effect due to the transverse motion of gravitational lenses and well known as the

Kaiser-Stebbins effect related to cosmic strings. Due to geometrical considerations, there is no significant three point correlation function, or a bispectrum, between the linear ISW effect and its non-linear counterpart. The correlation between the non-linear ISW effect and the kinetic SZ effect is again zero due to geometry associated with the line of sight and divergence of the momentum density field. The non-linear ISW contribution can be potentially used as a probe of the transverse velocity of dark matter halos such as galaxy clusters, however, due to the small contribution to temperature fluctuations of order few tenths of μK , extracting useful measurements on velocities will be challenging.

ACKNOWLEDGMENTS

We are grateful to Wayne Hu for useful discussions. We thank Ravi Sheth and his collaborators for providing us with an early draft of their paper on a halo model description of the velocity and momentum density fields and for useful conversations. We also thank Albert Stebbins for his encouragement of this work. A.C. was supported by a NASA grant NAG5-10840 at Chicago and by the Fairchild foundation at Caltech.

-
- [1] L. Knox, Phys. Rev. D, **52** 4307 (1995); G. Jungman, M. Kamionkowski, A. Kosowsky and D.N. Spergel, Phys. Rev. D, **54** 1332 (1995); J.R. Bond, G. Efstathiou and M. Tegmark, MNRAS, **291** L33 (1997); M. Zaldarriaga, D.N. Spergel and U. Seljak, Astrophys. J., **488** 1 (1997); D.J. Eisenstein, W. Hu and M. Tegmark, Astrophys. J., **518** 2 (1999)
 - [2] W. Hu, N. Sugiyama and J. Silk, Nature, **386**, 37 (1997)
 - [3] R. K. Sachs and A. M. Wolfe, Astrophys. J., **147** 73 (1967)
 - [4] M. J. Rees and D. N. Sciama, Nature, **519**, 611 (1968)
 - [5] R. J. Scherrer and E. Bertschinger, Astrophys. J. **381**, 349 (1991); R. K. Sheth and B. Jain, MNRAS, **285** 231 (1997); U. Seljak, MNRAS, **318** 203 (2000); C.-P. Ma and J. N. Fry, Astrophys. J., **543** 503 (2000); A. Cooray and W. Hu, Astrophys. J., **548** 7 (2001); R. Scoccimarro, R. Sheth, L. Hui and B. Jain, Astrophys. J., **546** 20 (2001)
 - [6] A. Cooray, 2001, Ph.D. thesis, University of Chicago, Chicago (2001); available from the U. of Chicago Crear Science Library or from the author; A. Cooray, Phys. Rev. D., in press (astro-ph/0105063)
 - [7] U. Seljak, Astrophys. J., **460** 549 (1996); also, R. Tuluie and P. Laguna, Astrophys. J., **445** 73 (1995); R. Tuluie, P. Laguna and P. Anninos, Astrophys. J., **463** 15 (1996)
 - [8] M. Birkinshaw and S. F. Gull, Nature, **302** 24 (1983)
 - [9] L. I. Gurvits and I. G. Mitrofanov, Nature, **324** 27 (1986); M. Birkinshaw, in Moving Gravitational Lenses, p. 59 eds. J. Moran, J. Hewitt and K. Y. Lo (Springer-Verlag: Berlin)
 - [10] N. Aghanim, S. Prunet, O. Forni and F. R. Bouchet, A&A, **334** 409 (1998)
 - [11] S. M. Molnar and M. Birkinshaw, Astrophys. J., **537** 542 (2000)
 - [12] N. Kaiser and A. Stebbins, Nature, **310** 2 (1984); A. Stebbins, Astrophys. J., **327** 584 (1988)
 - [13] P. J. E. Peebles, The Large-Scale Structure of the Universe, (Princeton: Princeton Univ. Press, 1980)
 - [14] P. T. P. Viana and A. R. Liddle MNRAS, **303** 535 (1999)
 - [15] E. F. Bunn and M. White, Astrophys. J., **480** 6 (1997)
 - [16] D. J. Eisenstein and W. Hu, Astrophys. J., **511** 5 (1999)
 - [17] D. Limber, Astrophys. J., **119** 655 (1954)
 - [18] J. M. Bardeen, Phys. Rev. D, **22** 1882 (1980)
 - [19] A. Cooray and W. Hu, Astrophys. J., **534**, 533 (2000)
 - [20] R. K. Sheth, A. Diaferio and I. Zehavi, MNRAS, submitted (2001); also, C.-P. Ma and J. N. Fry, preprint, astro-ph/0106342
 - [21] W. Hu, Astrophys. J., **529** 12 (1999)
 - [22] A. Cooray and W. Hu, Astrophys. J., **554** 56 (2001)
 - [23] R. A. Sunyaev and Ya. B. Zel'dovich, MNRAS, **190** 413 (1980)
 - [24] U. Seljak, Astrophys. J., **463** 1 (1996); M. Zaldarriaga and U. Seljak, Phys. Rev. D, **58** 023003 (1998); W. Hu, Phys. Rev. D, **62** 043007 (2000); W. Hu and A. Cooray, Phys. Rev. D, **63** 023504 (2001)
 - [25] A. Cooray, W. Hu and M. Tegmark, Astrophys. J., **540** 1 (2000)
 - [26] E. Komatsu and D. N. Spergel, Phys. Rev. D, **63** 063002 (2001); L. Wang and M. Kamionkowski, Phys. Rev. D, **61** 063504 (1999); A. Gangui and J. Martin, MNRAS, **313** 323 (2000); X. Luo and D. N. Schramm, Phys. Rev. Lett., **71** 1124 (1994); X. Luo Astrophys. J., **427** 71 (1994); T. Falk, R. Rangarajan and M. Frednicki, Astrophys. J. Lett., **403** L1 (1993);
 - [27] D. N. Spergel and D. M. Goldberg Phys. Rev. D, **59**, 103001 (1999)
 - [28] J. P. Ostriker and E. T. Vishniac, Nature, **322**, 804 (1986); E. T. Vishniac, Astrophys. J., **322**, 597 (1987);
 - [29] C. Da-Ming, X.-P. Wu and D.-R. Jiang, Astrophys. J., **544** 1 (2000)

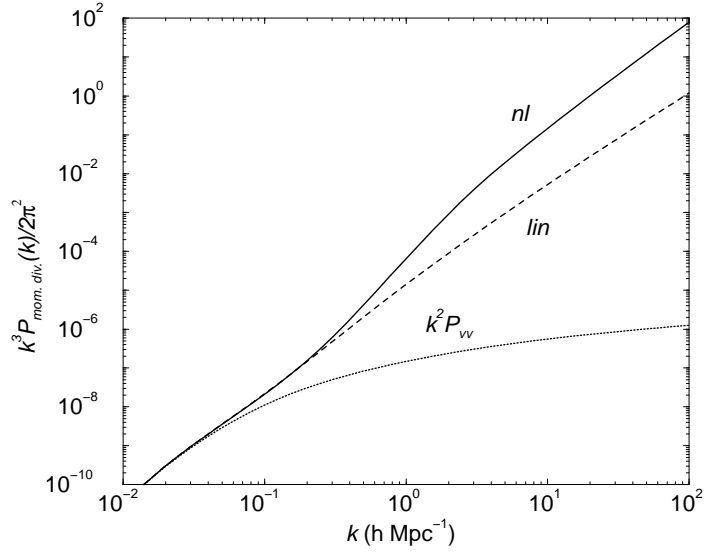


FIG. 1. The power spectrum of the divergence of the momentum density field, $P_{\delta\delta}(k)$. Here, we show the contribution due to the divergence of the velocity field and the extension to the non-linear regime using equation 20.

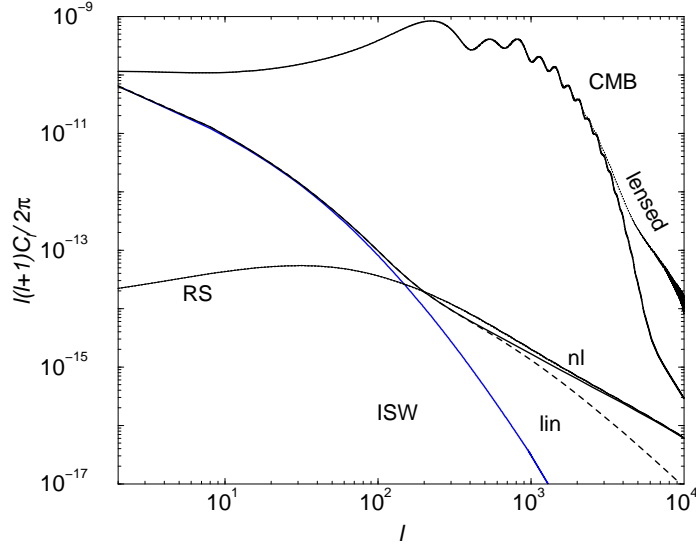


FIG. 2. The angular power spectrum of the full ISW effect, including non-linear contribution. The contribution called Rees-Sciama (RS) shows the non-linear extension, though for the total contribution, the cross term between the momentum field and the density field leads to a slight suppression between l of 100 and 1000. The curve labeled “nl” is the full non-linear contribution while the curve labeled “lin” is the contribution resulting from the momentum field under the second order perturbation theory.

- [30] W. Hu and A. Cooray, Phys. Rev. D, Phys. Rev. D, **63**, 023504 (2001).
- [31] D. M. Goldberg and D. N. Spergel, Phys. Rev. D, **59** 103002 (1999);
- [32] J. Navarro, C. Frenk and S. D. M. White, Astrophys. J., **462**, 563 (1996).
- [33] J. S. Bullock, T. S. Kolatt, Y. Sigad, MNRAS, in press, astro-ph/9908159 (2000); Y. P. Jing, Astrophys. J., **535**, 30 (2000)
- [34] J. E. Carlstrom, M. Joy and L. Grego, Astrophys. J., **456**, L75 (1996); M. Jones, R. Saunders, P. Alexander et al., Nature, **365**, 320 (1993)
- [35] U. Seljak and M. Zaldarriaga, Astrophys. J., preprint (astro-ph/9907554) (2001)
- [36] M. G. Haehnelt and M. Tegmark, MNRAS, **279**, 545 (1996)

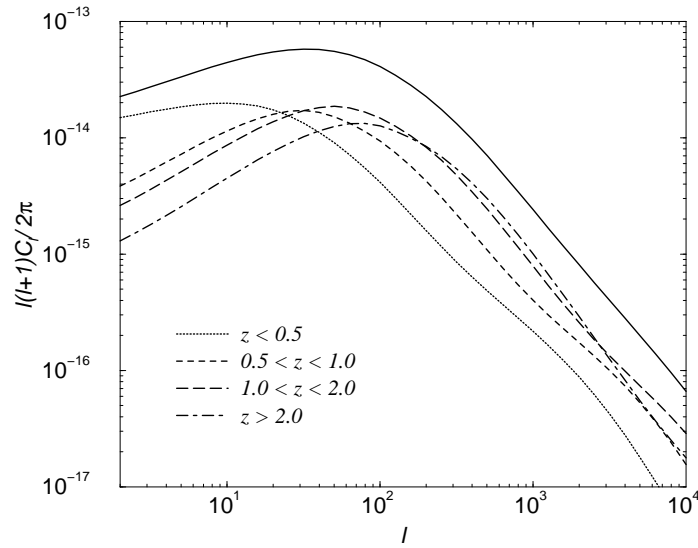


FIG. 3. The redshift dependence of the non-linear ISW contribution. Here, we break contributions at z less than 0.5 (dotted line), between 0.5 and 1.0 (dashed line), between 1.0 and 2.0 (long dashed line), and for redshifts greater than 2 (dot-dashed line). As shown, most of the contributions arise at a redshift of ~ 1 , leading to the peak in power at $l \sim 100$ and a sharp decrease thereafter.

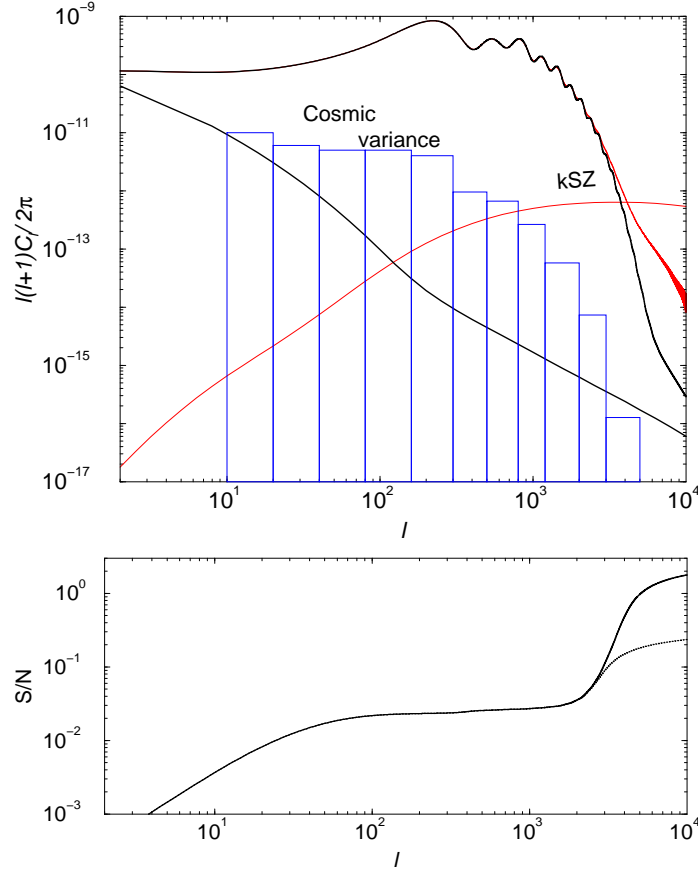


FIG. 4. (Top): The total ISW contribution compared with cosmic variance due to primary anisotropies. As shown, contributions are far below the cosmic variance and the non-linearities are not likely to impact the upcoming measurements of cosmological parameters from CMB data. At small angular scales, where the non-linear contributions are well above the sample variance, other secondary effects, such as the kinetic SZ, dominate the temperature fluctuations. (bottom) cumulative signal-to-noise for the detection of the non-linear ISW power spectrum, in the presence of the SZ thermal effect (dotted line) and not (solid line), and for an all sky experiment with no detector noise contribution.

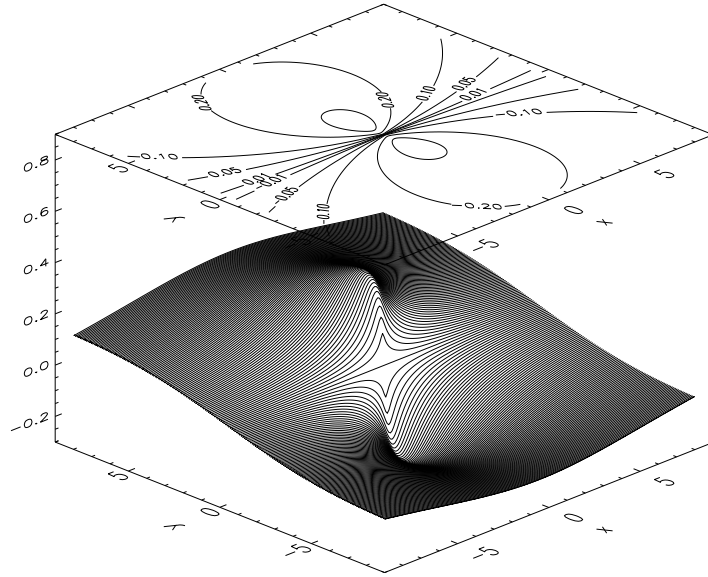


FIG. 5. The contribution due to the non-linear ISW effect for a cluster of mass $5 \times 10^{14} M_{\odot}$ with a transverse velocity of 100 km sec^{-1} across the line of sight. The temperature fluctuations produce a distinct dipolar pattern on the sky and are of order few tenths of micro Kelvin. Here, x and y coordinates are in terms of the scale radius of the cluster, based on a NFW profile.

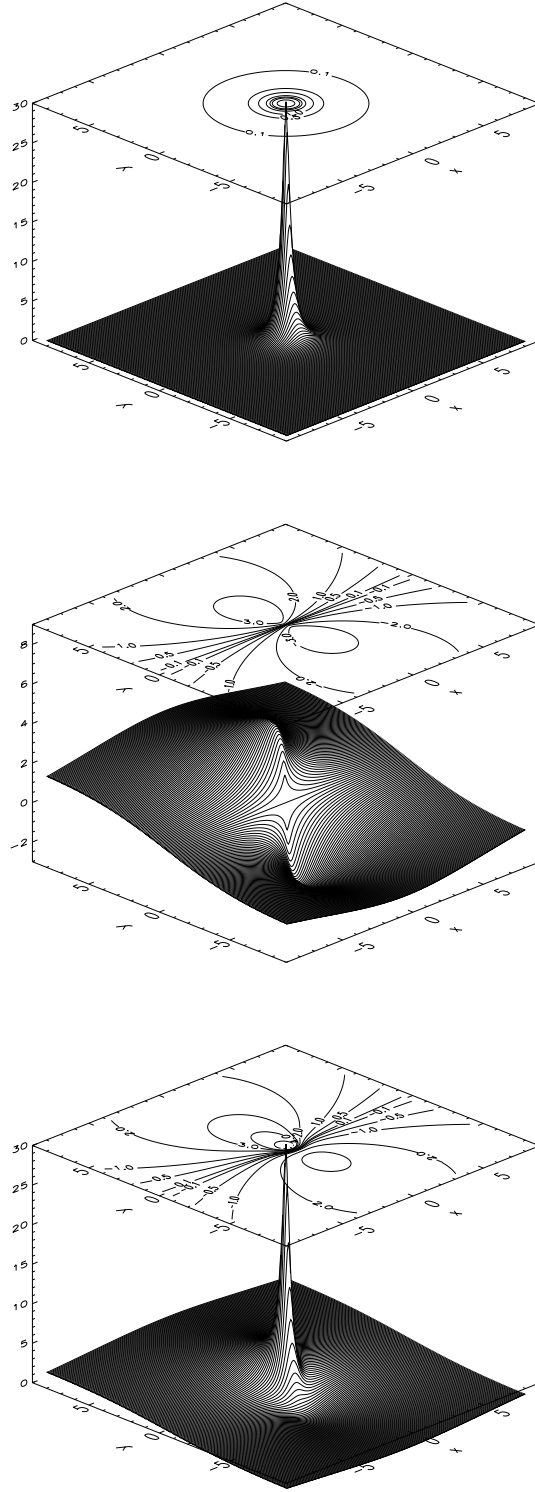


FIG. 6. Temperature fluctuations due to clusters. Top: kinetic SZ effect, middle: lensing of CMB primary temperature fluctuations, and bottom: the total contribution from kinetic SZ, lensing and transverse velocities. We use the same cluster as shown in figure 5.

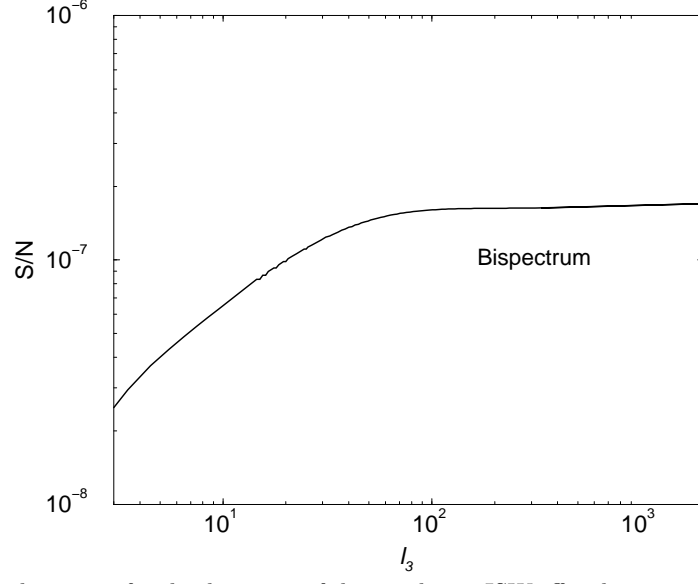


FIG. 7. The cumulative signal-to-noise for the detection of the non-linear ISW effect bispectrum as a function of the multipole l_3 .

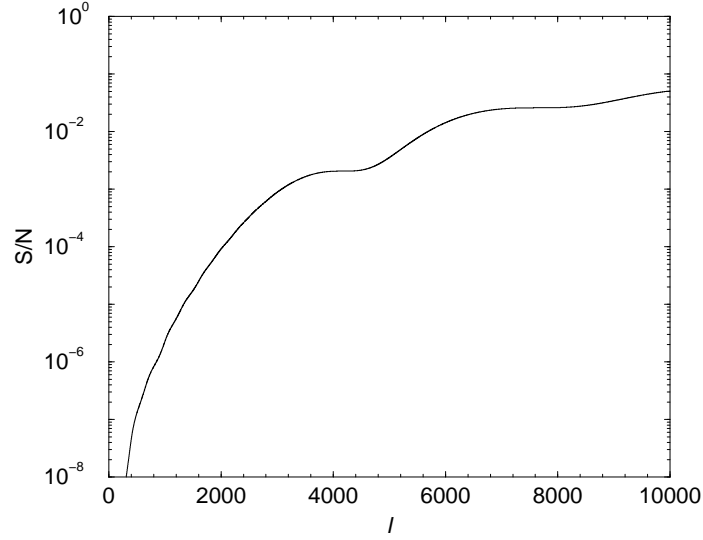


FIG. 8. The signal-to-noise for the detection of the non-linear ISW effect. The galaxy cluster considered here is the one in figure 5